Title

High-Fidelity Archeointensity Results for the Late Neolithic Period From Central China

Journal
Geophysical Research Letters, 47(10)

ISSN
0094-8276

Authors

Cai, Shuhui
Tauxe, Lisa
Wang, Weilin
et al.

Publication Date
2020-05-28

DOI
10.1029/2020gl087625

High-fidelity archeointensity results for the late Neolithic Period from central China

Shuhui Cai[1], Lisa Tauxe[2], Weilin Wang[3], Chenglong Deng[1,6], Yongxin Pan[4,6], Liping Yang[5], Huafeng Qin[1]

[1]State Key Laboratory of Lithospheric Evolution, Institute of Geology and Geophysics, Chinese Academy of Sciences, Beijing 100029, China;

[2]Scripps Institution of Oceanography, University of California, San Diego, La Jolla, CA 92093-0220, USA;

[3]College of History and Culture, Shanxi University, Taiyuan 030006, China;

[4]Key Laboratory of the Earth and Planetary Physics, Institute of Geology and Geophysics, Chinese Academy of Sciences, Beijing 100029, China;

[5]Shaanxi Provincial Institute of Archeology, Xi'an 710001, China

[6]College of Earth and Planetary Sciences, University of Chinese Academy of Sciences, Beijing 100049, China

Corresponding author: S. Cai (caishuhui@mail.iggcas.ac.cn)

Key points:

- 64 high-fidelity archeointensities were obtained from a late Neolithic site in central China
- New results record a fast field variation from ~55 to ~90 ZAm^2 between ~3500-3000 BCE and a new archeomagnetic jerk around ~3300 BCE
- An updated version of Chinese archeointensity reference curve (Archint_China2) was released for future application

Abstract

Archeomagnetism focuses on exploring high-resolution variations of the geomagnetic field over hundreds to thousands of years. In this study, we carried out a comprehensive study of chronology, absolute and relative paleointensity on a late Neolithic site in central China. Ages of the samples are constrained to be ~3500–3000 BCE, a period when available paleointensity data are sparse. We present a total of 64 high-fidelity absolute paleointensities, demonstrating the field varied quickly from ~55 to ~90 ZAm^2 between ~3500–3000 BCE. Our results record a new archeomagnetic jerk around 3300 BCE, which is probably non-dipolar origin. The new results provide robust constraints on global geomagnetic models. We calculated a revised Chinese archeointensity reference curve for future application. The variations of absolute and relative paleointensity versus depth show good consistency, reinforcing the reliability of our results. This new attempt of combining absolute and relative paleointenstiy provides a useful tool for future archeomagnetic research.

Plain language summary

The geomagnetic field is generated in the Earth's liquid outer core; its behavior can provide us information on the Earth's interior and help us understand processes deep in the planet we live on. The magnetic field surrounds the Earth and acts like an umbrella protecting the planet from strong solar winds, and thus the geomagnetic behavior can affect life on the Earth. Understanding the evolution of the geomagnetic field allows us to learn about the Earth in the past and can help us predict what will happen in the future. The geomagnetic field includes both dipolar and non-dipolar components, with the former related to global and the latter to regional features. Studying regional geomagnetic variations from different areas is essential for outlining regional features and global distributions of the field. In this study, we carried out archeomagnetic research on a late Neolithic archeological site in central China. The high-fidelity results fill a gap of the present data set in both space and time, and thus refine both the regional and global geomagnetic models significantly. The

newly released Chinese archeointensity reference curve in this study can be used for regional geomagnetic comparison as well as for archeological dating in this region.

1. Introduction

The geomagnetic field is one of the Earth's fundamental properties with a history of at least ~3.5 Ga (Biggin et al., 2011). It is a window into the deep interior of the Earth (Aubert et al., 2013; Bono et al., 2019; Davies & Constable, 2018) and may play a key role in evolution of life on the Earth (Lin et al., 2017). Baked archeological materials provide us an efficient way to explore detailed geomagnetic variations during the Holocene. Archeomagnetic studies in various areas contribute significantly to understanding of regional features and global distributions of the field. A number of regional reference curves (Cai et al., 2017a; Gallet et al., 2015; Goguitchaichvili et al., 2018; Gómez-Paccard et al., 2016; Hervé et al., 2013a, 2013b; Kovacheva et al., 2014; Tema & Kondopoulou, 2011) and global geomagnetic models (Constable et al., 2016; Nilsson et al., 2014; Pavón-Carrasco et al., 2014) have been established based partly or entirely on archeomagnetic data. In addition to regional comparisons, the established geomagnetic reference curves have applications in archeomagnetic dating (Hervé & Lanos, 2018; Peters et al., 2017).

The longevity of Chinese civilization and the abundance of archeological artifacts make archeomagnetic studies within China promising. New progress has been made in Chinese archeomagnetism in recent years (Cai et al., 2014, 2015, 2016, 2017a, 2017b) after ~20 years' quiescence. However, the recent studies are mainly from eastern China (Figure 1) and concentrated in the past 5 kyr. Data from other parts of China and older time periods are sparse. In this study, we focus on a late Neolithic archeological site in central China, whose age can be controlled through multiple dating techniques. The results fill gaps of the present data set in both space and time, and thus refine both the regional and global geomagnetic models significantly.

2. Archeological background and sampling

The site studied in this paper is located at Xi'an of Shanxi province, central China

(GPS: 34^{o}28.175’N, 109^{o}0.903’E) (Figure 1a) and named after the nearby village Yang-guan-zhai (YGZ). The YGZ site is a large habitation surrounded by a roughly square moat with a perimeter of ~2 km. Relics excavated from the moat were estimated to belong to Miaodigou culture in the late Neolithic Period according to their archeological characteristics, *e.g.*, typology and decoration of excavated potteries.

A segment at the southwest corner of the moat was excavated and two symmetrical sections of ~5.5 m including 16 cultural layers were exposed (Figure 1b and c), where the south and north section were named S1 and S2, respectively. Sediments through the section are generally silty sand and can be divide into four approximate parts (Figure 1b), which are greyish-yellow sand (part I), loose greyish-green sand mixed with ash (part II), transition between loose and compact sediments (part III) and compact silty sand (part IV). We collected a number of artifacts, mostly pottery sherds, from each layer of both sections for absolute paleointensity studies (Figure 1d). We measured the depth below the ground surface of each sample. Additional samples were collected from the storehouse for S1 in the intervals in which limited or no samples were found *in situ*.

Oriented sediments also were collected from S1 to investigate paleosecular variation, including relative paleointensity (Figure 1e). We collected block samples from different depth along the section by shaving a horizontal plane and marking the north direction of each sample with a magnetic compass. Samples were then removed from the wall. A total of 26 hand samples were collected through S1 and cut into 2-cm cubic specimens in the lab. Nomenclature of the samples is explained in Text S1 of the supporting information (SI).

Charcoals were collected for radiocarbon dating wherever available through both sections. A total of 14 charcoals (10 from S1 and 4 from S2) were collected (Figure S1).

3. Methods

3.1 Radiocarbon dating

In order to constrain ages of the samples investigated here, the 14 charcoal samples were sent to the AMS Laboratory of University of Arizona for ^{14}C analysis. The accelerator mass spectrometry dating method was adopted. Detailed information for the experimental procedure can be found in Jull et al. (2003).

3.2 Rock magnetism

We conducted rock magnetic studies, including hysteresis loops, first order reversal curves (FORCs) and variation of magnetization versus temperature (M−T), on selected potteries and sediments to detect properties of the magnetic minerals. Details of these experiments were described in Text S2 in SI.

3.3 Absolute paleointensity

A total of 107 samples with 69 from S1 and 38 from S2 were prepared for absolute paleointensity experiments by preparing them into 355 specimens with 226 from S1 and 129 from S2. Among these specimens, 76 were processed at the Paleomagnetism and Geochronology Laboratory (PGL), Institute of Geology and Geophysics, Chinese Academy of Sciences (IGGCAS) while the other 279 were measured in the Paleomagnetism Laboratory of the Scripps Institution of Oceanography (SIO), University of California, San Diego, USA.

An ‘IZZI’ protocol (Yu et al., 2004) was employed for the paleointensity experiment. Temperature intervals were set from 100 °C to 20 °C, larger at low temperatures and smaller at high temperatures. The pTRM checks were inserted at every other step to detect potential alteration during heating (Coe et al., 1978). The laboratory field of 30 μT was applied along +z axis of the specimens at PGL and -z at SIO, with a precision better than 0.1 μT for the ‘in field’ steps. The anisotropy of TRM (ATRM) was determined on each successful specimen in the intensity experiment, including eight steps of baseline, +x, +y, +z, -x, -y, -z and +x (Veitch et al., 1984). The last step is for an alteration check. A total TRM was used for calculating the anisotropy tensors to correct the specimen intensities for the effect of anisotropy. The cooling rate correction experiment includes four steps: baseline, fast cooling, slow cooling and a second fast cooling for an alteration check (Genevey & Gallet, 2002). The slow-cooling step takes ~6 and ~12 hours for the MMTDSC oven at PGL and for the laboratory-built oven at SIO, respectively. Specimens processed in the French furnace at PGL need not to be corrected for cooling rate effect because they were cooled naturally. More details about the experimental procedure are described in Text S3 of the SI.

3.4 Relative paleointensity

The oriented hand samples were further cut into 2-cm cubes (76 in total) for relative paleointensity study. Bulk susceptibilities (κ) of these cubes were measured by a Kappa-bridge magnetometer with an applied field of 300 A/m under a frequency of 875 Hz. After measuring their natural remanent magnetizations (NRMs), specimens were step-wise demagnetized in an alternating field (AF) demagnetizer with an interval of 5 mT up to 30 mT and 10 mT up to 80 mT. Anhysteretic remanent magnetizations (ARMs) were imparted to specimens under a bias field of 0.05 mT in an alternating peak field of 100 mT and step-wise AF demagnetized under peak field of 20 to 80 mT with an interval of 10 mT. Isothermal remanent magnetizations (IRMs) were imparted to specimens with a field of 1 T using a pulse magnetizer and then AF demagnetized following the same procedure for ARMs. All the original remanent magnetizations and remanences remaining after each step were measured with the 2G 760 SQUID magnetometer. These experiments were conducted at PGL.

4. Results

4.1 Radiocarbon dating

Among the analyzed 14 charcoal samples, 5 of them dissolved during pretreatment while the other 9 yielded results. The detailed dating information of all samples is listed in Table S1. The measured dates were calibrated by the atmospheric curve of IntCal13 (Reimer et al., 2013) with the software OxCal v4.3.2 (Bronk Ramsey, 2017). Unfortunately, ages of the samples fall on a plateau of the calibration curve (Figure

S2), which limits the age resolution through the section. Calibrated ages were plotted versus depth in Figure S3a, where ages of samples from different depths are not distinguishable from each other except Y2xra1 records an older age than others. We conducted a depth correction on these ages using the 'Sequence' function incorporated in OxCal by assuming deeper samples to be older (Bronk Ramsey, 1995). Depth-calibrated ages are shown in red dots in Figure S3b. Ages of samples between two radiocarbon dates were constrained by the younger boundary of the radiocarbon date above and older boundary of the date below (blue squares in Figure S3b). Ages of bottom samples from the sections were constrained by the younger boundary of the deepest radiocarbon date and the older boundary of archeological estimation for the site. Ages of the studied samples were constrained to ~3500–3000 BCE by combination of radiocarbon and archeological dating.

4.2 Rock magnetism

The hysteresis and FORCs (Harrison & Feinberg, 2008) results indicate magnetic carriers are mainly low-coercivity magnetic minerals with mixed superparamanetic (SP) and single-domain (SD) particles for both potteries and sediments (Figure S4a-f and g-l). M–T curves for potteries show good consistency between heating and cooling curves, with curie temperatures (T_cs) around 550 °C (Figure S4m-n). This indicates thermally-stable (titano)magnetite to be dominant magnetic minerals in these potteries, which are suitable for absolute paleointensity study. M–T curves for sediments show some alteration after heating (Figure S4o-r), with T_cs around 580–590 °C, which indicates magnetite is dominant among the samples. Rock magnetic results for sediments from different parts of the section show minimal discrepancy, which supports the feasibility of relative paleointensity study on these samples.

4.3 Absolute paleointensity

We adopted a modified version of the stringent criteria 'CCRIT' put forward by Cromwell et al. (2015), with deviation angle (DANG) less than 6° instead of 10° in

‘CCRIT’, unanchored maximum angular deviation (MAD$_{free}$) less than 6° instead of 5° and standard deviation of sample-average intensity less than 5 μT instead of 4 μT. The other parameters are the same as ‘CCRIT’ (Table S2). Each parameter is explained briefly in the table caption and detailed description can be found in Shaar & Tauxe (2013) and Paterson et al. (2014). The parameter $|\vec{k}|$ was first defined by Paterson (2011), describing the absolute curvature of the data points obtained during the paleointensity experiment. Cromwell et al. (2015) modified it somewhat ($|\overrightarrow{k'}|$) to restrict the calculation to those data points used for calculating the paleointensity. Paterson (2011) suggested a criterion of $|\vec{k}| \leq 0.164$ can yield reliable paleointensities according to their simulated paleointensity results, but also mentioned that it is very strict, especially for many natural specimens, and may exclude reliable results in some cases. Therefore, we modified the criterion for $|\overrightarrow{k'}|$ slightly: if there is at least one specimen with $|\overrightarrow{k'}| \leq 0.164$, we accept sister specimens from the same sample with $|\overrightarrow{k'}| > 0.164$ yet obtaining comparable paleointensities. We attempt to guarantee the reliability of paleointensities and save more data simultaneously by modifying the ‘CCRIT’ criteria slightly. Data were analyzed with the ‘Thellier GUI’ program (Shaar & Tauxe, 2013) incorporated in the PmagPy software package (Tauxe et al., 2016). A total of 64 out of 107 samples (221 out of 355 specimens) passed the selection criteria. Results of the accepted samples and specimens are listed in Table S3 and Table S4, respectively. Representative Arai plots (Nagata et al., 1963) yielding accepted paleointensities are shown in Figure 2a and b, showing straight lines and single components with limited viscous remanent magnetizations (VRMs). Alterations of the accepted specimens during the anisotropy correction experiments are all less than 10% (90% of them less than 5%) while those during cooling rate correction are all less than 5% except one being 9%. The extent of anisotropy correction for ~58% of the accepted specimens are less than 10% while the others have strong anisotropic effect with maximum correction reaches 62%. The cooling rate correction is generally less than 10% (Table S4). Accepted paleointensities, which vary from ~30 to ~50 μT, were plotted versus depth in Figure 3a through the section. Intensities of samples collected *in situ* from S1, S2 and from the storehouse are shown with different symbols; these are generally consistent with each other, reinforcing the reliability of our data.

4.4 Relative Paleointensity

The measured parameters of oriented sediments, including step-wise NRM, κ, ARM and IRM, through the section are shown in Figure S5. Variation in the trends of these parameters is very consistent. κ versus ARM and IRM were divided into four groups according to lithology in Section 1 (Figure S6). Distributions are slightly different among groups but all show good linear relationship, demonstrating grain sizes of the sediments within each group are generally uniform, satisfying one of the most basic requirements for relative paleointensity study (Tauxe, 1993). Relative paleointensities were calculated following the pseudo-Thellier approach of Tauxe et al. (1995), normalizing NRM with ARM and IRM selecting the remanence between 20–80 mT (Figure 3b and c). AF demagnetization data of oriented sediments were analyzed with the 'Demag GUI' function incorporated in PmagPy. The criteria of $MAD_{free} \leq 6°$, DANG ≤ 6° and $n \geq 9$ were used to constrain the data quality, where n is the number of data points used in calculating the characteristic remanent magnetization (ChRM). A total of 51 out of 76 specimens pass the criteria (Table S5). Representative successful specimens are shown in Figure 2c and d; these have a characteristic component after removal of a soft component by 15 mT on the Zijderveld plot (Zijderveld, 1967). Accepted declinations and inclinations were plotted versus depth in Figure 3d and e, where the former vary between ~330° and ~10° and the latter vary from ~36° to ~64° through the section.

5. Discussion

We carried out an absolute paleointensity study on potteries from two sections in a moat and obtained 64 high-fidelity paleointensities for the time period of ~3500–3000 BCE. We employed stringent criteria modified from ‘CCRIT’ (Cromwell et al., 2015) to ensure data quality. The reliability of the intensities is also cross checked by results from independent sections, *e.g.*, S1 *in situ*, S1 from the storehouse and S2 *in situ*, and confirmed by the consistency among them (Figure 3a).

We compared variations of absolute paleointensity, relative paleointensity (NRM/ARM and NRM/IRM), declination and inclination through the section (Figure 3). The variation trends between absolute and relative paleointensity in each part of the four generally show good consistency, especially at certain depths of abrupt change, marked by orange dashed lines. It is worth mentioning that pottery ages at a given depth must be older than the deposition age of the sediments at the same depth since potteries were made first and then buried in the strata. Therefore, geomagnetic signals recorded by potteries at a given depth should be synchronous with those recorded by deeper sediments. Interestingly, we can indeed identify this pattern in our results (see dashed lines in Figure 3). The consistency between absolute and relative paleointensity provide us two key points: Firstly, it reinforces the reliability of our absolute paleointensity data with independent evidence; Secondly, the results convince us that sediments from archeological sites as in this study can sometimes record geomagnetic signals although their depositional contexts are more human-involved compared to sediments from natural sites. These suggest possibilities for future study about similar archeological sites.

Virtual axial dipole moments (VADMs) of our new data are plotted together with published data from 1980s–1990s (Huang et al., 1998; Shaw et al., 1995; Wei et al., 1982, 1986) and from recent years (Cai et al., 2014, 2015, 2017a) in China (Figure 4). Data from studies published prior to 2000 were selected with the criteria of $N_{min} \geq 3$, $\sigma_{age} \leq 500$ yr and $\sigma_B \leq 5$ μT or 10%, while data published since were reanalyzed with the same criteria used in this study. The recently published data from Korea (Hong et al., 2013) and Japan (Yu, 2012) are also shown on the plot. We recalculated the

Chinese archeointensity reference curve (Archint_China2) with new data from this study and our reanalyzed data published in recent years, following the bootstrap-running average method described in Cai et al. (2017a)— resampling 1,000 times at each data point and then applying a running average with a time window of 200 y shifted by 10 y on the resampled dataset. The calculated curve is attached in Table S6 for readers' convenience. When comparing Archint_China2 to predictions at the center of China (35°N, 105°E) from global models pfm9k.1a (Nilsson et al., 2014) and ARCH10k.1 (Constable et al., 2016), large discrepancies can be found for certain time periods (*e.g.*, 3000–2000 BCE). Our local reference curve provides more detail and the underlying data can be used to refine the global models.

Our new results suggest that the field varied quickly, from ~55 to ~90 ZAm^2, between 3500 and 3000 BCE, which is also accompanied by variations of declinations (~330°–10°) and inclinations (~36°–64°) of the oriented sediments. Although our new data could not provide a high-resolution variation curve of the geomagnetic field as the ages fall on a plateau of the calibration curve, we nonetheless constrained the variation range of the field over ~500 years with many new high-quality points (see insert in Figure 4).

Our new results, combined with published data from adjacent period, outline a maximum of the field intensity around 3300 BCE, which is possibly a new archeomagnetic jerk. Archeomagnetic jerks were first reported in Europe (Gallet et al., 2003), representing a moderate field behavior between 'geomagnetic jerks' (Mandea et al., 2010) and 'geomagnetic spikes' (Ben-Yosef et al., 2009). The archeomagnetic jerks recorded in Europe were characterized by intensity maxima as well as abrupt directional changes. Unfortunately, published archeodirectional data from a similar time in this area are too sparse to provide convincing evidence. Further study on archeodirection should be carried out in the future. However, the intensity maxima (recorded by potteries from ~420–480 cm), accompanied by convincing directional changes in the companion sediments (~440–510 cm) recorded by our new data together constitute reasonably strong evidence of the existence of an archeomagnetic jerk at ~3300 BCE in China.

In order to characterize the global context of this new possible jerk, we compiled data from west-mid Asia and Europe, where enough data from this time period are available from Geomagia50.v3.3 database (Brown et al., 2015), and compared them to east Asia (Figure 5). Neither data from west-mid Asia (Figure 5c) nor from Europe (Figure 5d) record such a clear jerk as in our data (Figure 5a), indicating this geomagnetic behavior is probably a regional feature of non-dipolar origin.

6. Conclusions

We conducted archeomagnetic studies on two excavated sections of a moat at the late Neolithic site YGZ in central China. Combined radiocarbon and archeological dating constrain ages of the studied samples to ~3500–3000 BCE. High-fidelity absolute paleointensities from 64 samples were acquired, whose reliability is ensured by stringent selection criteria and further confirmed by consistency between two independent sections as well as coincidence of variation between absolute and relative paleointensity through the section. Our new intensities indicate that the field varied quickly, from ~55 to ~90 ZAm^2, between 3500 and 3000 BCE. Our results record a new archeomagnetic jerk around 3300 BCE in China, which is probably a regional (non-dipolar) feature. The regional reference curve of archeointensity in China, Archint_China2, is an update combining new data from this study with reanalyzed data published in recent years. Future studies are recommended to use this new version of reference curve for regional geomagnetic field comparison. Our new results fill a gap of the present Chinese archeointensity data set and provide robust constraints for global models. The new attempt of combining absolute and relative paleointenstiy in this study shed light on future archeomagnetic research.

7. Acknowledgements

We thank Quan Hua for his help during analysis of radiocarbon dating data, Nicolas Santiago and Rashida Doctor for doing part of the measurements, and Liang Yi for assisting in sampling in the field. We are grateful to Courtney Sprain and an anonymous reviewer for their constructive comments on early manuscript. This work was supported by NSFC grants (41974077, 41621004 and 41888101) and NSF grants (EAR1520674 and EAR1547263) to LT. Shuhui Cai thanks support from CAS Pioneer Hundred Talents Program. Original data related to this paper have been uploaded to the MagIC database (earthref.org/MagIC/16357) and will be available on acceptance of the manuscript.

References

Aubert, J., Finlay, C. C., & Fournier, A. (2013), Bottom-up control of geomagnetic secular variation by the Earth's inner core. *Nature*, *502*(7470), 219-223.

Ben-Yosef, E., Tauxe, L., Levy, T. E., Shaar, R., Ron, H., & Najjar, M. (2009), Geomagnetic intensity spike recorded in high resolution slag deposit in Southern Jordan. *Earth and Planetary Science Letters*, *287*(3-4), 529-539.

Biggin, A. J., de Wit, M. J., Langereis, C. G., Zegers, T. E., Voûte, S., Dekkers, M. J., et al. (2011), Palaeomagnetism of Archaean rocks of the Onverwacht Group, Barberton Greenstone Belt (southern Africa): Evidence for a stable and potentially reversing geomagnetic field at ca. 3.5 Ga. *Earth and Planetary Science Letters*, *302*(3), 314-328.

Bono, R. K., Tarduno, J. A., Nimmo, F., & Cottrell, R. D. (2019), Young inner core inferred from Ediacaran ultra-low geomagnetic field intensity. *Nature Geoscience*, *12*(2), 143-147.

Bronk Ramsey, C. (1995), Radiocarbon calibration and analysis of stratigraphy: the OxCal program. *Radiocarbon*, *37*(2), 425-430.

Bronk Ramsey, C. (2017), Methods for summarizing radiocarbon datasets. *Radiocarbon*, *59*(6), 1809-1833.

Brown, M. C., Donadini, F., Korte, M., Nilsson, A., Korhonen, K., Lodge, A., et al. (2015), GEOMAGIA50.v3: 1. general structure and modifications to the archeological and volcanic database. *Earth Planets and Space*, *67*(83), doi: 10.1186/s40623-40015-40232-40620.

Cai, S., Jin, G., Tauxe, L., Deng, C., Qin, H., Pan, Y., et al. (2017a), Archaeointensity results spanning the past 6 kiloyears from eastern China and implications for extreme behaviors of the geomagnetic field. *Proceedings of the National Academy of Sciences of the United States of America*, *114*(1), 39-44.

Cai, S., Tauxe, L., Paterson, G. A., Deng, C., Pan, Y., Qin, H., et al. (2017b), Recent advances in Chinese archeomagnetism. *Frontiers in Earth Science*, *5*(92), doi: 10.3389/feart.2017.00092.

Cai, S., Chen, W., Tauxe, L., Deng, C., Qin, H., Pan, Y., et al. (2015), New constraints on the variation of the geomagnetic field during the late Neolithic period: Archaeointensity results from Sichuan, southwestern China. *Journal of Geophysical Research: Solid Earth*, *120*(4), 2056-2069.

Cai, S., Tauxe, L., Deng, C., Pan, Y., Jin, G., Zheng, J., et al. (2014), Geomagnetic intensity variations for the past 8 kyr: New archaeointensity results from Eastern China. *Earth and Planetary Science Letters*, *392*, 217-229.

Cai, S., Tauxe, L., Deng, C., Qin, H., Pan, Y., Jin, G., et al. (2016), New archaeomagnetic direction results from China and their constraints on palaeosecular variation of the geomagnetic field in Eastern Asia. *Geophysical Journal International*, *207*, 1332-1342.

Coe, R. S., Grommé, S., & Mankinen, E. A. (1978), Geomagnetic paleointensities from radiocarbon-dated lava flows on Hawaii and the question of the Pacific nondipole low. *Journal of Geophysical Research: Solid Earth*, *83*(B4), 1740-1756.

Constable, C., Korte, M., & Panovska, S. (2016), Persistent high paleosecular variation activity in southern hemisphere for at least 10 000 years. *Earth and Planetary Science Letters*, *453*, 78-86.

Cromwell, G., Tauxe, L., Staudigel, H., & Ron, H. (2015), Paleointensity estimates from historic and modern Hawaiian lava flows using glassy basalt as a primary source material. *Physics of the Earth and Planetary Interiors*, *241*, 44-56.

Davies, C. J., & Constable, C. G. (2018), Searching for geomagnetic spikes in numerical dynamo simulations. *Earth and Planetary Science Letters*, *504*, 72-83.

Gallet, Y., Genevey, A., & Courtillot, V. (2003), On the possible occurrence of ‘archaeomagnetic jerks’ in the geomagnetic field over the past three millennia. *Earth and Planetary Science Letters*, *214*(1-2), 237-242.

Gallet, Y., Molist Montaña, M., Genevey, A., Clop García, X., Thébault, E., Gómez Bach, A., et al. (2015), New Late Neolithic (c. 7000–5000 BC) archeointensity data from Syria. Reconstructing 9000 years of archeomagnetic field intensity variations in the Middle East. *Physics of the Earth and Planetary Interiors*, *238*, 89-103.

Genevey, A., & Gallet, Y. (2002), Intensity of the geomagnetic field in Western Europe over the past 2000 years: new data from French ancient pottery. *Journal of Geophysical Research*, *107*(2285), doi: 10.1029/2001JB000701.

Goguitchaichvili, A., Ruiz, R. G., Pavón-Carrasco, F. J., Contreras, J. J. M., Arechalde, A. M. S., & Urrutia-Fucugauchi, J. (2018), Last three millennia Earth’s Magnetic field strength in Mesoamerica and southern United States: Implications in geomagnetism and archaeology. *Physics of the Earth and Planetary Interiors*, *279*, 79-91.

Gómez-Paccard, M., Osete, M. L., Chauvin, A., Pavón-Carrasco, F. J., Pérez-Asensio, M., Jiménez, P., et al. (2016), New constraints on the most significant paleointensity change in Western Europe over the last two millennia. A non-dipolar origin? *Earth and Planetary Science Letters*, *454*, 55-64.

Harrison, R. J., & Feinberg, J. M. (2008), FORCinel: An improved algorithm for calculating first-order reversal curve distributions using locally weighted regression smoothing. *Geochemistry, Geophysics, Geosystems*, *9*(5), Q05016, doi:05010.01029/02008GC001987.

Hervé, G., & Lanos, P. (2018), Improvements in archaeomagnetic dating in Western Europe from the late Bronze to the late Iron Ages: An alternative to the problem of the hallstattian radiocarbon plateau. *Archaeometry*, *60*(4), 870-883.

Hervé, G., Chauvin, A., & Lanos, P. (2013a), Geomagnetic field variations in Western Europe from 1500BC to 200AD. Part I: Directional secular variation curve. *Physics of the Earth and Planetary Interiors*, *218*, 1-13.

Hervé, G., Chauvin, A., & Lanos, P. (2013b), Geomagnetic field variations in Western Europe from 1500BC to 200AD. Part II: New intensity secular variation curve. *Physics of the Earth and Planetary Interiors*, *218*, 51-65.

Hong, H., Yu, Y., Lee, C. H., Kim, R. H., Park, J., Doh, S.-J., et al. (2013), Globally strong geomagnetic field intensity circa 3000 years ago. *Earth and Planetary Science Letters*, *383*, 142-152.

Huang, X. G., Li, D. J., & Wei, Q. Y. (1998), Secular variation of geomagnetic intensity for the last 5000 years in China-comparison between the southwest and other parts of China. *Chinese Journal of Geophysics*, *41*, 385-396.

Jull, A. J. T., Burr, G. S., Beck, J. W., Donahue, D. J., Biddulph, D., Hatheway, A. L., et al. (2003), Accelerator mass spectrometry at Arizona: geochronology of the climate record and connections with the ocean. *Journal of Environmental Radioactivity*, *69*(1-2), 3-19.

Kovacheva, M., Kostadinova-Avramova, M., Jordanova, N., Lanos, P., & Boyadzhiev, Y. (2014), Extended and revised archaeomagnetic database and secular variation curves from Bulgaria for the last eight millennia. *Physics of the Earth and Planetary Interiors*, *236*, 79-94.

Lin, W., Paterson, G. A., Zhu, Q., Wang, Y., Kopylova, E., Li, Y., et al. (2017), Origin of microbial biomineralization and magnetotaxis during the Archean. *Proceedings of the National Academy of Sciences of the United States of America*, *114*(9), 2171-2176.

Mandea, M., Holme, R., Pais, A., Pinheiro, K., Jackson, A., & Verbanac, G. (2010), Geomagnetic jerks: rapid core field variations and core dynamics. *Space Science Reviews*, *155*(1-4), 147-175.

Nagata, T., Arai, Y., & Momose, K. (1963), Secular variation of the geomagnetic total force during the last 5000 years. J. Geophys. Res., 68, 5277-5281.

Nilsson, A., Holme, R., Korte, M., Suttie, N., & Hill, M. (2014), Reconstructing Holocene geomagnetic field variation: new methods, models and implications. *Geophysical Journal International*, *198*(1), 229-248.

Paterson, G. A. (2011), A simple test for the presence of multidomain behavior during paleointensity experiments. *Journal of Geophysical Research*, *116*(B10), doi:

10.1029/2011jb008369.

Paterson, G. A., Tauxe, L., Biggin, A. J., Shaar, R., & Jonestrask, L. C. (2014), On improving the selection of Thellier-type paleointensity data. *Geochemistry, Geophysics, Geosystems*, *15*(4), 1180-1192.

Pavón-Carrasco, F. J., Osete, M. L., Torta, J. M., & De Santis, A. (2014), A geomagnetic field model for the Holocene based on archaeomagnetic and lava flow data. *Earth and Planetary Science Letters*, *388*, 98-109.

Peters, I., Tauxe, L., & Ben-Yosef, E. (2017), Archaeomagnetic dating of pyrotechnological contexts: a case study for copper smelting sites in the Central Timna Valley, Israel. *Archaeometry*, *60*(3), 554-570.

Reimer, P. J., Bard, E., Bayliss, A., Beck, J. W., Blackwell, P. G., Ramsey, C. B., et al. (2013), IntCal13 and Marine13 radiocarbon age calibration curves 0–50,000 years cal BP. *Radiocarbon*, *55*(4), 1869-1887.

Shaar, R., & Tauxe, L. (2013), Thellier GUI: An integrated tool for analyzing paleointensity data from Thellier-type experiments. *Geochemistry, Geophysics, Geosystems*, *14*(3), 677-692.

Shaw, J., Yang, S., & Wei, Q. Y. (1995), Archaeointensity variations for the past 7500 years evaluated from ancient Chinese ceramics. *Journal of Geomagnetism and Geoelectricity*, *47*, 59-70.

Tauxe, L. (1993), Sedimentary records of relative paleointensity of the geomagnetic field: Theory and practice. *Reviews of Geophysics, 31*, 319-354.

Tauxe, L., Pick, T., & Kok, Y.S. (1995), Relative paleointensity in sediments: a pseudo-Thellier approach. *Geophysical Research Letters, 22*, 2885-2888.

Tauxe, L., Shaar, R., Jonestrask, L., Swanson-Hysell, N. L., Minnett, R., Koppers, A. A. P., et al. (2016), PmagPy: Software package for paleomagnetic data analysis and a bridge to the Magnetics Information Consortium (MagIC) Database. *Geochemistry, Geophysics, Geosystems*, *17*(6), 2450-2463.

Tema, E., & Kondopoulou, D. (2011), Secular variation of the Earth's magnetic field in the

Balkan region during the last eight millennia based on archaeomagnetic data. *Geophysical Journal International*, *186*(2), 603-614.

Veitch, R. J., Hedley, I. G., & Wagner, J. J. (1984), An investigation of the intensity of the geomagnetic field during Roman times using magnetically anisotropic bricks and tiles. *Archives Des Sciences*, *37*(3), 359–373.

Wei, Q., Li, D., Cao, G., Zhang, W., & Wang, S. (1982), Intensity of the geomagnetic field near Loyang, China between 500 BC and AD 1900. *Nature*, *296*(5859), 728-729.

Wei, Q., Li, D., Cao, G., Zhang, W., & Wei, S. F. (1986), The total intensity of geomagnetic field in southern China for the period from 4500 B.C. to A.D. 1500. *Journal of Geomagnetism and Geoelectricity, 38*, 1311-1322.

Yu, Y. (2012), High-fidelity paleointensity determination from historic volcanoes in Japan. *Journal of Geophysical Research*, *117*(B8), B08101, doi: 08110.01029/02012JB009368.

Yu, Y., Tauxe, L., & Genevey, A. (2004), Toward an optimal geomagnetic field intensity determination technique. *Geochemistry, Geophysics, Geosystems, 5*, doi: 10.1029/2003GC000630.

Zijderveld, J. D. A. (1967), A.C. demagnetization of rocks: analysis of results. In: Collinson, D., Creer, K., Runcorn, S. (Eds.), Methods in Paleomagnetism. *ELsevier, Amsterdam*, pp: 254–286.

Figure 1. Site locality and field photos. (a) Locations of Chinese archeological sites. Red star represents location of this study. China_new pub (purple squares) means locations of data published in recent years since 2014. China_old pub (black solid circles) means locations of data published in the 1980s and 1990s. (b) and (c) Field photos of the south and north section. (d) and (e) Sampling photos of unoriented potteries and oriented sediments from the south section.

Figure 2. Representative absolute paleointensity and AF demagnetization results. (a) and (b) Examples of accepted Arai plots and the relative orthogonal projections (a1 and b1) and NRM remaining (blue)-pTRM gained curves (red) (a2 and b2). Numbers on the Arai plot and orthogonal projections are temperature steps in centigrade (°C). The green line on each plot shows the temperature section used to calculate the paleointensity. Photos of the samples are shown as inserts. (c) and (d) Representative orthogonal projections of accepted specimens. Red solid circles/blue squares represent projections on horizontal/vertical plane. The green line on each plot shows the temperature section used to calculate the characteristic direction. Numbers on the diagrams are AF steps in mT. Related plots of equal area (c1 and d1) and normalized magnetization versus AF steps (c2 and d2) are shown as inserts.

Figure 3. Comparison of absolute and relative paleointensity. (a) Absolute paleointensities from S1 (black solid and open circles) and S2 (purple solid circles). (b) and (c) ARM and IRM normalized relative paleointensities. Remanence intervals of 20–80 mT were used. (d) and (e) Declinations and inclinations versus depth. Symbols in green/ blue/ red/ dark in (b-e) represent samples from part I / II/ III/ IV of Section 1, respectively. Orange dashed lines between (a) and (b) show correlations between absolute and relative paleointensities.

Figure 4. Comparison of VADMs in this study to published data in Eastern Asia and predictions from global models. Red stars are data from this study. Amplified plot is shown as insert. Black solid circles are data published in the 1980s and 1990s after selection. Purple squares are our reanalyzed data published in recent years since 2014.

Cyan hexagons/blue pentagons are published data in Japan (Yu, 2012)/Korea (Hong et al., 2013) in recent years. The grey and yellow lines are predictions from global models of ARCH10k.1 (Constable et al., 2016) and pfm9k.1a (Nilsson et al., 2014) at the center of China (35°N, 105°E). The orange line is the updated Chinese archeointensity reference curve.

Figure 5. Regional comparison of the archeomagnetic jerk around ~3300 BCE. (a) Distribution map of compiled data. (b) Compilation of data from east Asia. Only data published in the recent years were included. (c) Compilation of data from west-mid Asia. (d) Compilation of data from Europe (between 40–60°N and 10°W–30°E). Data from the Geomagia50.v3.3 database were selected with the criteria of $N_{min} \geq 3$, $\sigma_{age} \leq 500$ yr and $\sigma_B \leq 5$ μT or 10%. The regional curves were calculated following the same technique for ArchInt_China.2. The cyan rectangles indicate age ranges of the archeomagnetic jerk in China.

Figure1.


(a)
50°N
40°N
30°N
20°N
70°E
80°E
90°E
100°E
110°E
120°E
130°E
● China_old pub
■ China_new pub
★ This study
(b) Section1
Ⅰ
170 cm
Ⅱ
315 cm
Ⅲ
410 cm
Ⅳ
(c) Section2
(d) Section1
unoriented pottery
(e) Section1
oriented sediment

Figure2.

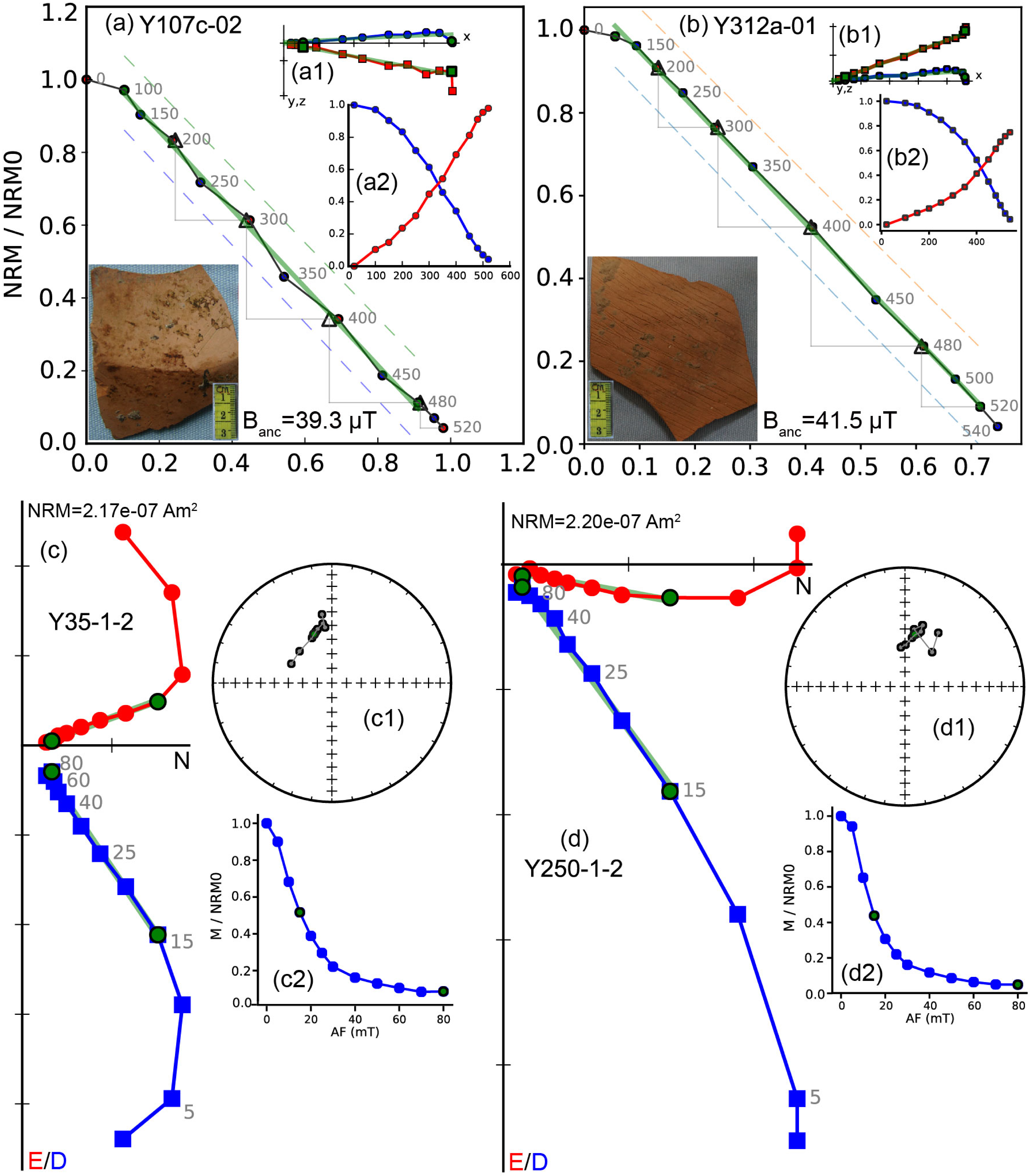
(a) Y107c-02
NRM / NRM0
1.2
1.0
0.8
0.6
0.4
0.2
0.0
0.0
0.2
0.4
0.6
0.8
1.0
1.2
0
100
150
200
250
300
350
400
450
480
520
(a1)
x
y,z
(a2)
1.0
0.8
0.6
0.4
0.2
0.0
0
100
200
300
400
500
600
cm
1
2
3
B_{anc}=39.3 μT
(b) Y312a-01
1.0
0.8
0.6
0.4
0.2
0.0
0.0
0.1
0.2
0.3
0.4
0.5
0.6
0.7
0
150
200
250
300
350
400
450
480
500
520
540
(b1)
x
y,z
(b2)
1.0
0.8
0.6
0.4
0.2
0.0
0
200
400
cm
1
2
3
B_{anc}=41.5 μT
NRM=2.17e-07 Am^2
(c)
Y35-1-2
N
80
60
40
25
15
5
(c1)
1.0
0.8
0.6
0.4
0.2
0.0
M / NRM0
(c2)
0
20
40
60
80
AF (mT)
E/D
NRM=2.20e-07 Am^2
N
80
40
25
15
5
(d1)
(d)
Y250-1-2
1.0
0.8
0.6
0.4
0.2
0.0
M / NRM0
(d2)
0
20
40
60
80
AF (mT)
E/D

Figure3.

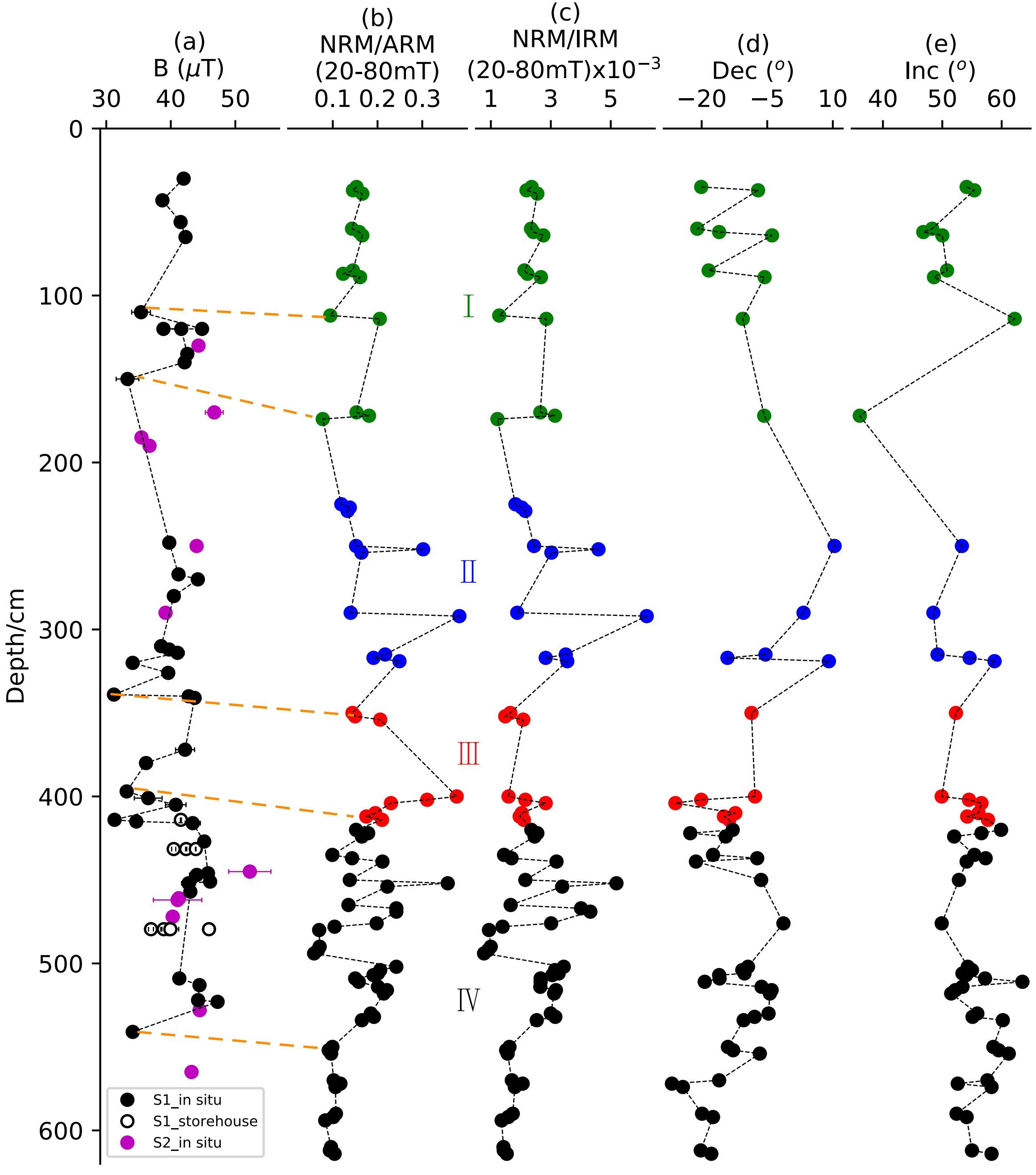
(a)
B (μT)
30
40
50
(b)
NRM/ARM
(20-80mT)
0.1
0.2
0.3
(c)
NRM/IRM
(20-80mT)x10^{-3}
1
3
5
(d)
Dec (^{o})
−20
−5
10
(e)
Inc (^{o})
40
50
60
Depth/cm
0
100
200
300
400
500
600
Ⅰ
Ⅱ
Ⅲ
Ⅳ
S1_in situ
S1_storehouse
S2_in situ

Figure4.

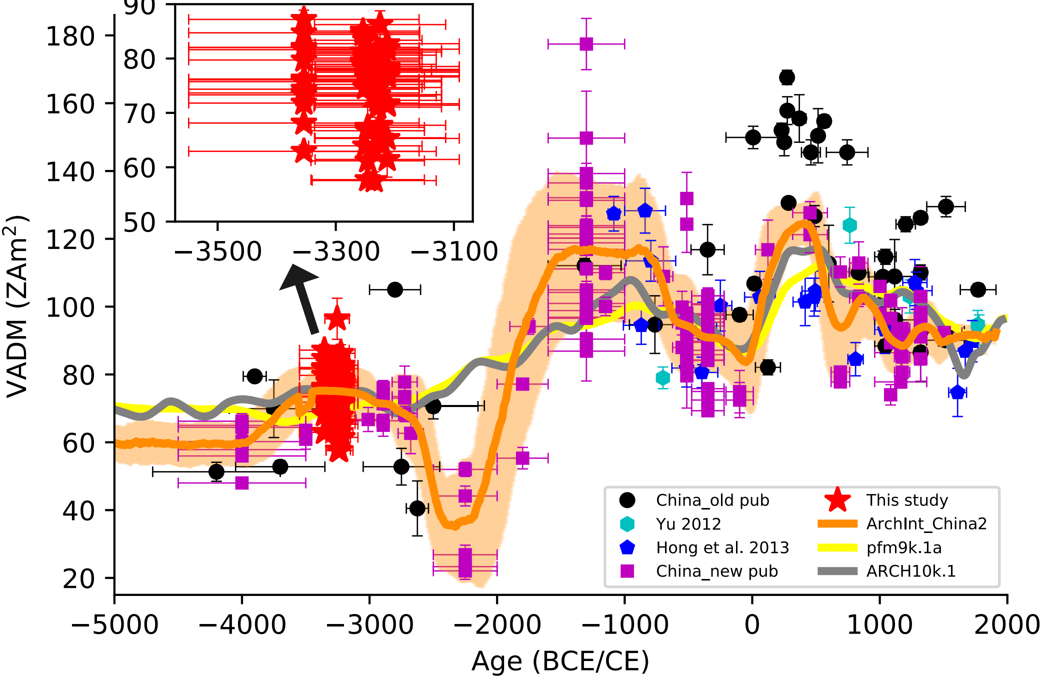
90
80
70
60
50
−3500
−3300
−3100
180
160
140
120
100
80
60
40
20
VADM (ZAm^2)
−5000
−4000
−3000
−2000
−1000
0
1000
2000
Age (BCE/CE)
China_old pub
Yu 2012
Hong et al. 2013
China_new pub
This study
ArchInt_China2
pfm9k.1a
ARCH10k.1

Figure5.

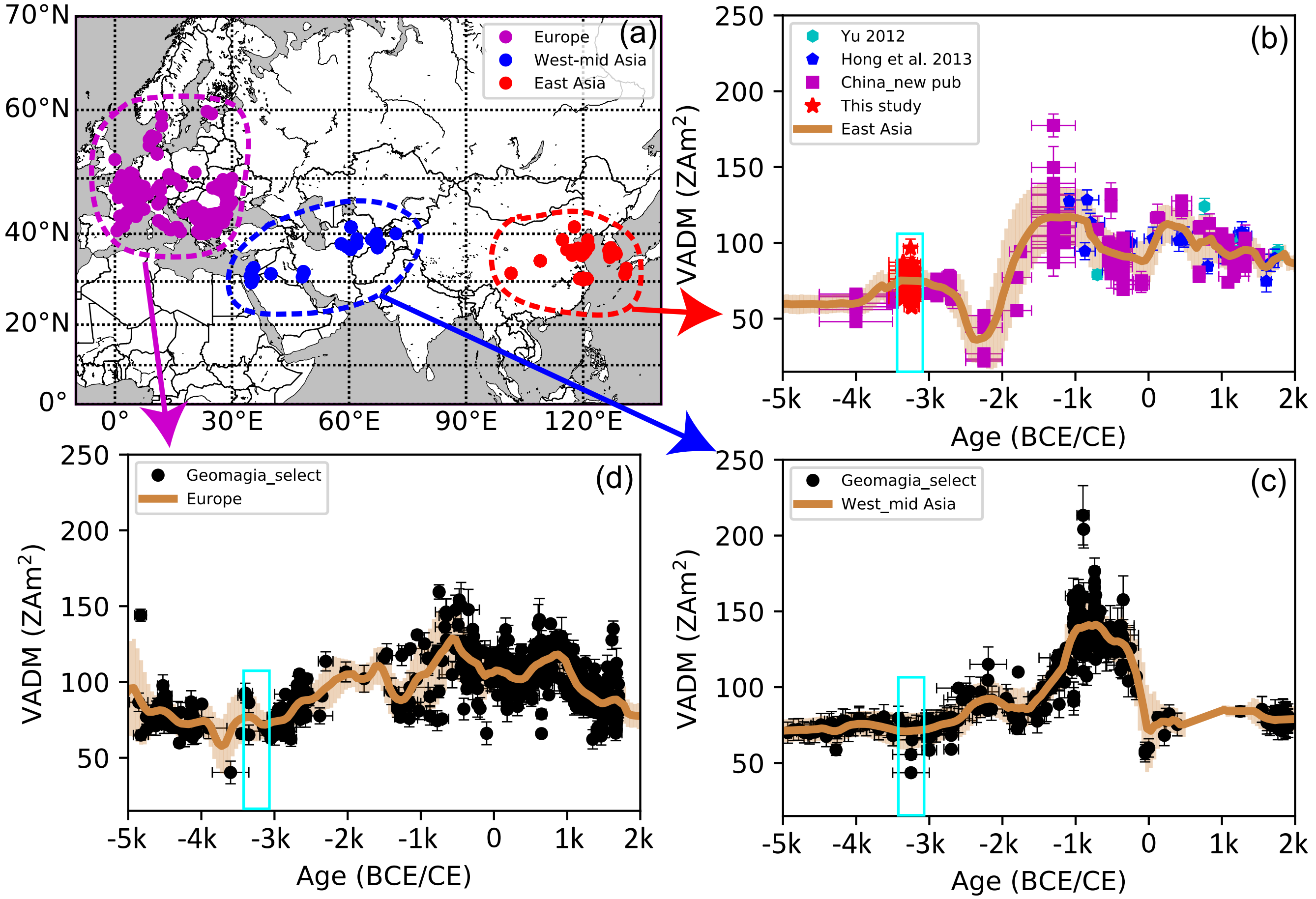
70°N
60°N
40°N
20°N
0°
0°
30°E
60°E
90°E
120°E
(a)
Europe
West-mid Asia
East Asia
(b)
Yu 2012
Hong et al. 2013
China_new pub
This study
East Asia
VADM (ZAm^2)
250
200
150
100
50
-5k
-4k
-3k
-2k
-1k
0
1k
2k
Age (BCE/CE)
(c)
Geomagia_select
West_mid Asia
VADM (ZAm^2)
Age (BCE/CE)
(d)
Geomagia_select
Europe
VADM (ZAm^2)
Age (BCE/CE)